applied sciences

MDPI

Article

Stability Analysis of Lane-Keeping Assistance System for Trucks under Crosswind Conditions

He Liu [1], Conghao Liu [1,*], Liang Hao [1] and Dongmin Zhang [2]

[1] School of Automobile and Traffic Engineering, Liaoning University of Technology, Jinzhou 121001, China; lhlngydx@126.com (H.L.); hl867438249@126.com (L.H.)
[2] BYD Auto Industry Company Limited, Shenzhen 518000, China; zhanghaorong@163.com
* Correspondence: qcxy_lch@lnut.edu.cn

Abstract: To enhance the control accuracy of lane-keeping assistance systems for trucks encountering crosswind-induced lateral deviations to improve the lateral stability of the vehicle, this study proposes a control strategy based on a linear quadratic regulator (LQR) using a path-tracking preview model. First, the lateral deviation is calculated using the path-tracking preview model. Then, an observer for the vehicle's sideslip angle is designed using a vehicle lateral tracking deviation model and a Kalman filter controller, and this is used to solve the deviation of the sideslip angle. Finally, a feedforward controller is designed based on the LQR controller and a linear two-degrees-of-freedom vehicle model to eliminate steady-state errors arising from LQR optimization, thereby obtaining the steering angle of the vehicle when subjected to crosswind conditions. Comparing the test results of the sideslip angle, yaw rate, and lateral acceleration demonstrates that this strategy effectively improves the control accuracy of lane-keeping under crosswind conditions. The proposed method is validated through hardware-in-the-loop experiments on a test bench, yielding results consistent with simulations.

Keywords: lane-keeping assistance; crosswind; linear quadratic regulator controller; hardware-in-the-loop experiments

Citation: Liu, H.; Liu, C.; Hao, L.; Zhang, D. Stability Analysis of Lane-Keeping Assistance System for Trucks under Crosswind Conditions. *Appl. Sci.* **2023**, *13*, 9891. https://doi.org/10.3390/app13179891

Academic Editors: Suchao Xie and Jerzy Jackowski

Received: 28 July 2023
Revised: 21 August 2023
Accepted: 30 August 2023
Published: 31 August 2023

1. Introduction

When vehicles are subjected to crosswinds during high-speed travel, their lateral positions can deviate, and this is especially true for box-shaped vehicles such as vans, large buses, and canvas-covered trucks. This deviation negatively affects the stability of vehicle handling, potentially leading to accidents. Addressing the issue of crosswind disturbances in high-speed vehicle operation is an important aspect of research on vehicle handling stability, and significant research has been conducted in this area. Zachiotis and Giakoumis [1] used Monte Carlo simulations to assess the impact of ambient wind on vehicle performance and emissions. Sekulic et al. [2] proposed a pure pursuit path-tracking method based on an eight-degrees-of-freedom model to address the influence of wind loads and floating bridge movements on the lateral stability of public buses in Bjørnafjord, Norway. Han et al. [3] developed a coupled vibration analysis of the wind, vehicle, and bridge to ensure the safety of vehicles on long-span bridges under crosswind conditions. Xu and Zhai [4] analyzed the problems of a vehicle–rail coupled system as a stochastic nonlinear system under the excitations of crosswind and random track irregularities. They proposed a stochastic analysis model for vehicle–rail coupling dynamics and random irregularities. Kim et al. [5] introduced a lateral disturbance compensation algorithm to reduce the driver steering effort under crosswind disturbances. Cioffi et al. [6] used a dynamic driving simulator to evaluate a driver's state when encountering crosswind and found that the driver's response typically exhibits an approximate delay of 0.25 s from the onset of crosswind stimuli. Tian et al. [7] developed a comprehensive evaluation framework for the lateral stability of vehicles under crosswind conditions, which provides guidance

for controlling adverse conditions and making road maintenance decisions. Although these methods have performed well in practical applications, the accuracy of their lateral deviation control is limited due to the lack of consideration of the influence of the vehicle's sideslip angle.

In modern society, traffic accidents continually occur, leading to increasing casualties. Surveys have shown that approximately 50% of traffic accidents are caused by vehicles deviating from their normal travel lane. To address the issue of vehicles unintentionally deviating from their intended travel path, researchers have begun to study the control strategies of lane-keeping assistance systems (LKASs). Bian et al. [8] proposed an advanced LKAS with two switchable auxiliary modes, namely the lane departure prevention and co-driver lane-keeping modes, to address the reliability issues of fully autonomous lane-keeping systems. Kim et al. [9] presented a torque overlay-based robust steering wheel angle control method for the lane-keeping systems of autonomous vehicles. Chen et al. [10] suggested a lane-keeping control method based on a Takagi–Sugeno fuzzy model to reduce the lateral deviation of vehicles. Zhang et al. [11] proposed a deep learning model to estimate the lateral distance between a vehicle and the lane boundary, providing an effective benchmark for road testing of LKASs. Zhou et al. [12] developed a driver-centric and neural-adaptive control-based LKAS to address traffic safety issues caused by vehicle departures from lanes. Wu et al. [13] developed a novel lane-keeping assistance method that applies additional yaw moments to electric vehicles and actively distributes the driving/braking torque to all four wheels for lane keeping. Han et al. [14] addressed the frequent lane departure issue in commercial vehicles and devised an LKAS based on an electro-hydraulic steering system. Lim et al. [15] designed an LKAS based on human driving data to prevent vehicle lane departures in situations with an unaware driver. Kővári et al. [16] introduced a reinforcement learning-based approach to address the lateral control problem of dynamic nonlinear vehicle models for lane-keeping tasks.

In summary, the current research on LKAS control strategies and crosswind issues mostly focuses on individual aspects or problems, without considering their interaction. Therefore, this study addresses the issue of low control accuracy when handling the lateral deviations of vehicles under crosswind conditions in the application of lane-keeping control systems. The LKAS control strategy based on the path-tracking preview algorithm and the LQR controller is proposed to improve the lateral stability of the vehicle.

2. Materials and Methods

2.1. Simulation Model

For vehicles with a LKAS, it is relatively easy to drive along the middle of the lane on a planned straight path. However, when the vehicle enters a curved road, in order to continue to remain in the middle of the lane, the vehicle will repeatedly adjust the steering angle, which can easily reduce the lateral stability of the vehicle, especially for larger trucks. When the vehicle encounters crosswind on a curved road, the stability will decrease even more severely. This study proposes a LKAS control strategy based on the path-tracking preview algorithm and the LQR controller, to improve the lateral stability of the vehicle. To achieve the control objectives, it is necessary to establish a reasonable vehicle dynamics model to describe the vehicle's motion state. Additionally, a path-tracking preview model is developed to determine the deviation between the vehicle and road centerline. Then, a feedforward controller is established using the linear quadratic regulator (LQR) algorithm and a linear two-degrees-of-freedom vehicle model, to eliminate steady-state errors generated during optimal control by the LQR algorithm, thereby further reducing the lateral deviation. Considering the influence of the vehicle's sideslip angle on lateral vehicle control, an observer for the sideslip angle is established based on the vehicle's lateral tracking deviation model and the Kalman filter algorithm. Using the yaw rate and lateral acceleration as the observation values, the deviation of the vehicle's sideslip angle is estimated. Finally, the LQR algorithm is used to optimize the estimated deviation

and obtain the driver's steering wheel angle, therefore improving the control accuracy of the lateral deviation.

2.1.1. Simulation Methods

As shown in Figure 1, the lateral deviation caused by crosswind is calculated by using the path-tracking preview algorithm through the road line information, the path trajectory provided by TruckSim, and the deviation of the driver's prediction point. Then, the lateral deviation, sideslip angle deviation, and yaw rate deviation are fused with the gain matrix calculated by the LQR algorithm to obtain a steering wheel angle, which is then added to the compensated steering angle obtained by the feedforward controller to calculate the final steering wheel angle, and this wheel angle is input to TruckSim. TruckSim will provide various parameters of the vehicle in motion to the algorithm built by Matlab/Simulink, such as yaw rate, lateral acceleration, front wheel angle, and deviation between path trajectory and driver's prediction point, and then a closed-loop control is formed. Finally, through hardware in the loop experiments, the proposed LKAS control strategy is used to control the vehicle driving in the middle of the road line, and experiments are conducted on three operating conditions: "without crosswind", "crosswind without LQR control", and "crosswind with LQR control", to verify the effectiveness of the LKAS control strategy.

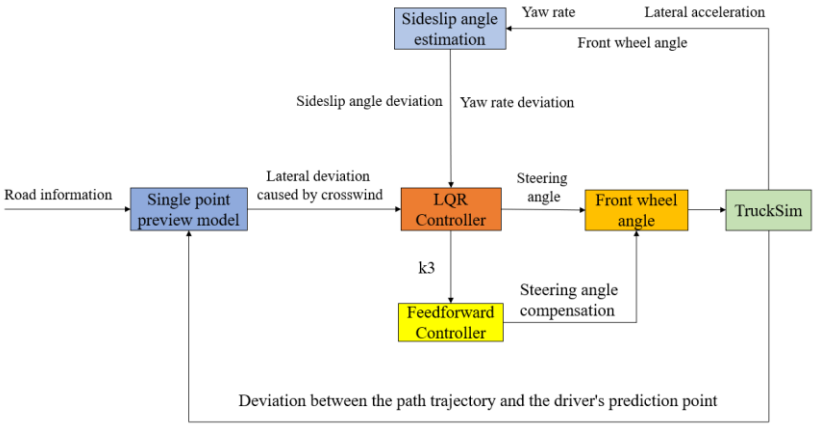

Figure 1. Control strategy flowchart for simulation.

2.1.2. Road Model and Crosswind

According to GB/T 41796-2022 [17], the test road is designed as a straight and curved composite road. In this study, the vehicle is driving straight in the first 4 s, then from 4 s to 20 s is the curved part, which is divided into fixed curvature and variable curvature. The curvature radius of the fixed curvature part is 500 m, the variable curvature part is the connection section of the straight and the fixed curvature part of the bend, and its curvature changes linearly with the length of the curve, gradually increasing from 0 to 0.002 m^{-1} (the rate of change is less than 4×10^{-5} m^{-2}). The test road is shown in Figure 2, where S_0, S_1, and S_2 are the straight part, the variable curvature part, and the fixed curvature part, respectively, the road width, d, is 10 m, and the road adhesion coefficient is 0.85.

Since the step crosswind has simple mathematical properties and permits analysis of the vehicle's response to a linearized equation of motion [18], in this study, a step crosswind was selected for simulation. Figure 2 presents the direction of the crosswind, where the wind velocity was 40 km/h. In the simulation, from t = 0~4 s, the vehicle was on a straight road; from t = 4~6 s, the vehicle was subjected to a crosswind for 2 s, and from t = 6 s to the end, the crosswind was removed from the simulation. Throughout the entire process, the relevant parameters of vehicle lateral stability will be observed.

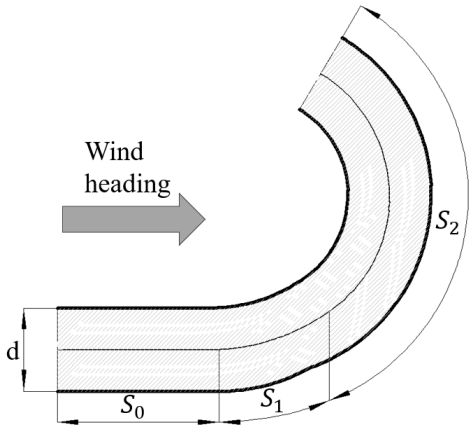

Figure 2. Road model drawing.

2.1.3. Linear Two-Degrees-of-Freedom Vehicle Dynamics Model

Since the LKAS primarily focuses on the lateral motion of the vehicle, an accurate vehicle lateral dynamics model is required. In this study, a linear two-degrees-of-freedom vehicle dynamics model was adopted, which includes the vehicle's lateral motion along the y-axis and yaw motion along the z-axis. The linear two-degrees-of-freedom vehicle model is illustrated in Figure 3.

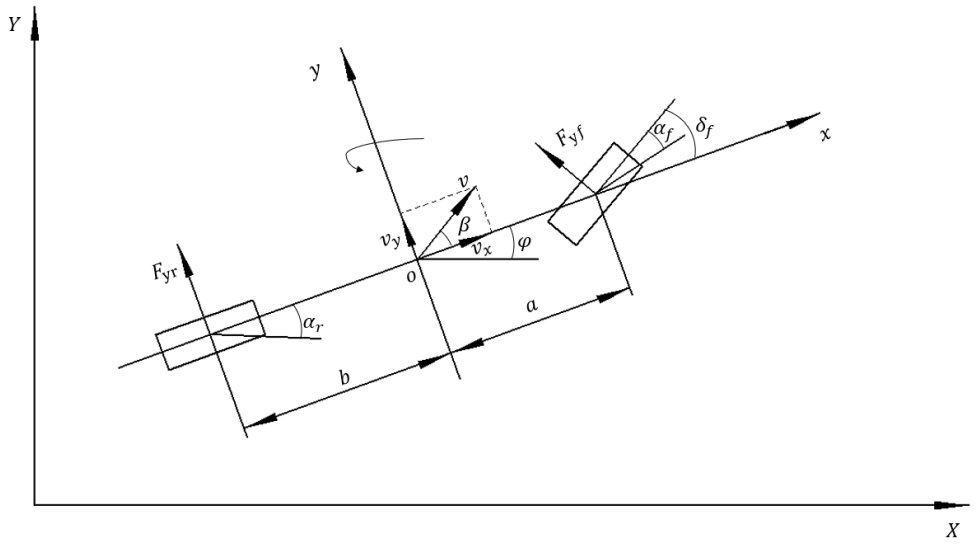

Figure 3. Linear two-degrees-of-freedom vehicle model.

First, the forces acting in the y-direction and the torques along the z-axis of the vehicle were analyzed to establish the equilibrium equations:

$$\begin{cases} F_y = m\left(\ddot{y} + v_x\ddot{\varphi}\right) \\ M_z = I\ddot{\varphi} \end{cases}, \tag{1}$$

where m, y, v_x, and φ are the mass, lateral displacement, longitudinal velocity, and yaw angle of the vehicle, respectively, and I is the moment of inertia of the vehicle along the z-axis.

Based on Figure 3, the resultant force acting on the vehicle in the y-direction and the moment around the center of mass can be obtained as:

$$\begin{cases} F_y = F_{yf}\cos\delta_f + F_{yr} \\ I\ddot{\varphi} = aF_{yf}\cos\delta_f - bF_{yr} \end{cases}, \tag{2}$$

where, F_{yf} and F_{yr} are the lateral reaction forces from the ground on the front and rear wheels, respectively, δ_f is the steering angle of the front wheels, and a and b are the distances from the vehicle's center of mass to the front and rear axles, respectively.

Considering that the lateral tire forces are approximately linearly related to the tire slip angles when the slip angles are small, the lateral force can be calculated using the following equation:

$$\begin{cases} F_{yf} = C_f \alpha_f \\ F_{yr} = C_r \alpha_r \end{cases}, \tag{3}$$

where C_f and C_r are the front and rear tire stiffnesses, respectively, and a_f and a_r are the front and rear tire slip angles, respectively.

Assuming that the steering angle is very small and approaches 1°, Equations (1)–(3) yield:

$$\begin{cases} m\left(\ddot{y} + v_x \ddot{\varphi}\right) = C_f \alpha_f + C_r \alpha_r \\ I\ddot{\varphi} = aC_f \alpha_f - bC_r \alpha_r \end{cases}. \tag{4}$$

Based on the linear two-degrees-of-freedom vehicle model and assuming small sideslip angles, the following equation can be obtained:

$$\begin{cases} \alpha_f = \frac{\dot{\varphi} a + v_y}{v_x} - \delta_f \\ \alpha_r = \frac{v_y - \dot{\varphi} b}{v_x} \end{cases}, \tag{5}$$

where v_y is the lateral velocity of the vehicle.

By combining Equations (1)–(5), the linear two-degrees-of-freedom dynamic model can be derived as:

$$\begin{bmatrix} \ddot{y} \\ \ddot{\varphi} \end{bmatrix} = \begin{bmatrix} \frac{C_f + C_r}{m v_x} & \frac{aC_f - bC_r}{m v_x} - v_x \\ \frac{aC_f - bC_r}{I v_x} & \frac{a^2 C_f + b^2 C_r}{I v_x} \end{bmatrix} \begin{bmatrix} \dot{y} \\ \dot{\varphi} \end{bmatrix} + \begin{bmatrix} -\frac{C_f}{m} \\ -\frac{aC_r}{I} \end{bmatrix} \delta_f. \tag{6}$$

2.1.4. Vehicle Lateral Tracking Deviation Model

To determine the lateral control deviation of the vehicle during autonomous driving, the established linear two-degrees-of-freedom vehicle dynamics model was transformed into a lateral tracking deviation model using coordinate transformation. The vehicle lateral tracking deviation model is illustrated in Figure 4.

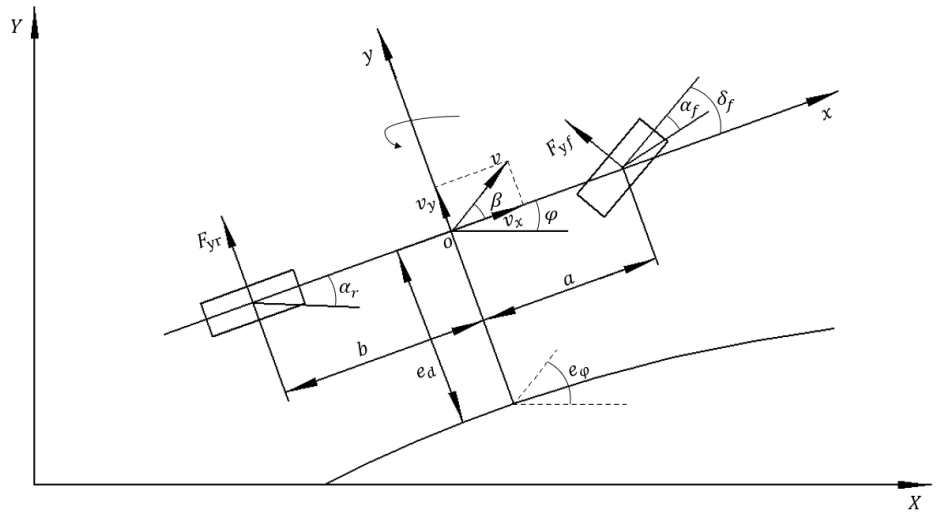

Figure 4. Vehicle lateral tracking deviation model.

First, the heading angle deviation, e_φ, is obtained as:

$$e_\varphi = \varphi_h - \varphi_r, \tag{7}$$

where φ_h and φ_r are the actual and ideal vehicle heading angles, respectively.

Next, based on Figure 4, the deviation of the vehicle's lateral acceleration, $\dot{e}_d$, can be derived as:

$$\dot{e}_d = v_x e_\varphi + v_y, \tag{8}$$

Finally, by combining Equations (7) and (8) with the linear two-degrees-of-freedom vehicle model, the vehicle lateral deviation model is obtained as:

$$\ddot{e}_d = \left(\frac{C_f + C_r}{m v_x}\right)\dot{e}_d + \left(-\frac{C_f + C_r}{m}\right)e_\varphi + \left(\frac{aC_f - bC_r}{m v_x}\right)\dot{e}_\varphi + \left(\frac{aC_f - bC_r}{m v_x} - v_x\right)\dot{\varphi}_r + \left(-\frac{C_f}{m}\right)\delta_f, \tag{9}$$

$$\ddot{e}_\varphi = \left(\frac{aC_f - bC_r}{I v_x}\right)\dot{e}_d + \left(-\frac{aC_f - bC_r}{I}\right)e_\varphi + \left(\frac{a^2C_f + b^2C_r}{I v_x}\right)\dot{e}_\varphi + \left(\frac{a^2C_f + b^2C_r}{I v_x}\right)\dot{\varphi}_r + \left(-\frac{aC_r}{I}\right)\delta_f. \tag{10}$$

Subsequently, the state-space equation is derived as:

$$\dot{X} = AX + BU + C\dot{\varphi}_r, \tag{11}$$

where $A = \begin{bmatrix} 0 & 1 & 0 & 0 \\ 0 & \frac{C_f+C_r}{mv_x} & -\frac{C_f+C_r}{m} & \frac{aC_f-bC_r}{mv_x} \\ 0 & 0 & 0 & 1 \\ 0 & \frac{aC_f-bC_r}{Iv_x} & -\frac{aC_f-bC_r}{I} & \frac{a^2C_f+b^2C_r}{Iv_x} \end{bmatrix}$, $X = \begin{bmatrix} e_d \\ \dot{e}_d \\ e_\varphi \\ \dot{e}_\varphi \end{bmatrix}$, $B = \begin{bmatrix} 0 \\ -\frac{C_f}{m} \\ 0 \\ -\frac{aC_r}{I} \end{bmatrix}$, $U = \begin{bmatrix} \delta_f \end{bmatrix}$,

and $C = \begin{bmatrix} 0 \\ \frac{aC_f-bC_r}{mv_x} - v_x \\ 0 \\ \frac{a^2C_f+b^2C_r}{Iv_x} \end{bmatrix}$.

2.1.5. Path-Tracking Preview Model

To describe the relationship between the vehicle and the road, an appropriate preview model must be established [19]. During path tracking, there exists a predicted deviation between the driver's line of sight and the centerline of the road, including the heading and lateral position deviations at the prediction point. The path-tracking preview model is illustrated in Figure 5.

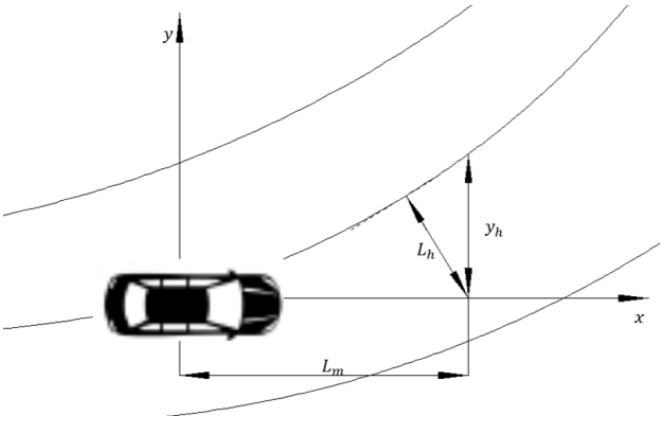

Figure 5. Path-tracking preview model.

Based on the geometric relationship in Figure 5, the following equation can be derived:

$$y_h = \frac{L_m}{\cos\left(\arcsin\left(\frac{L_h}{L_m}\right)\right)}, \tag{12}$$

where y_h is the lateral deviation, L_m is the preview distance, and L_h is the deviation between the path trajectory and the driver's prediction point. Considering the issue of insufficient vehicle steering, a PID (proportional integral derivative) controller was employed to optimize the lateral error and address this problem.

2.2. LKAS Control Strategy

2.2.1. LQR Controller

The main objective of the LQR controller is to determine the optimal control gains to achieve optimal control of the system [20]. The discrete state-space equation is obtained by applying the midpoint and forward Euler methods to discretize the state and control variables:

$$X(k+1) = A_T X(k) + B_T U(k), \tag{13}$$

where $A_T = \left(E - \frac{AT}{2}\right)^{-1}\left(E + \frac{AT}{2}\right)^{-1}$, $B_T = BT$, E is the identity matrix, $X(k)$ is the state variable of the system at time k, and $U(k)$ is the control variable required by the system at time k.

To improve the control performance, a target function is assumed:

$$J = \sum_k^{\infty}\left(X_k^T Q X_k + U_k^T Y U_k\right), \tag{14}$$

where X_k is the system state variable, U_k is the system control variable, and Q and Y are the weighted matrix coefficients for the system state and control variables, respectively. The problem now is to find the control law such that the cost function (14) is minimized under the constraint conditions.

The feedback controller for the LQR controller is:

$$U(k) = -KX(k), \tag{15}$$

where $K = \left(Y + B_T^T P B_T^{-1}\right)^{-1} B_T^T P A_T$ is the gain matrix of the feedback controller, in which P is the positive definite solution to the Riccati equation. The Riccati equation is as follows:

$$P = Q - A_T^T P B_T\left(Y + B_T^T P B_T\right)^{-1} B_T^T P A_T + A_T^T P A_T. \tag{16}$$

By incorporating the combined deviation matrix, e_r, of the lateral position and heading angle deviations, δ_f, into the system state variable and the front wheel steering angle into the control variable, the LQR control law based on the front wheel steering angle is derived as:

$$\begin{cases} \delta_f(k) = -Ke_r(k) \\ K = \begin{bmatrix} k_1 & k_2 & k_3 & k_4 \end{bmatrix} \\ e_r = \begin{bmatrix} e_d & \dot{e}_d & e_\varphi & \dot{e}_\varphi \end{bmatrix} \end{cases}, \tag{17}$$

where K is the gain matrix of the LQR controller and e_r is the combined deviation matrix.

2.2.2. Feedforward Controller Based on LQR

To eliminate the steady-state errors that occur when optimizing the front wheel steering angle using the LQR controller [21], Equation (11) is combined with Equations (15) and (17) to obtain the steady-state errors of the system:

$$\dot{e}_r = Ae_r + C\dot{\varphi}_r + B\left(\delta_f - Ke_r\right). \tag{18}$$

Observing Equation (18), it can be noticed that even when $\dot{e}_r = e_r = 0$, steady-state errors still exist. Therefore, an appropriate front wheel steering angle needs to be determined to set $e_r = 0$. By solving Equation (18), the following expression is obtained:

$$\delta_f = \frac{\dot{\varphi}_r}{v_x}\left[a + b - bk_3 - \frac{mv_x^2}{a+b}\left(\frac{b}{C_f} + \frac{a}{C_r}k_3 - \frac{a}{C_r}\right)\right], \tag{19}$$

where k_3 is the gain coefficient in the first row and third column of gain matrix K.

2.2.3. Kalman Filter

The Kalman filter is a recursive minimum variance estimation method that efficiently manages real-time signals in control systems [22]. It is widely used in linear systems, and the discrete and continuous forms of these systems can be mutually converted. Suppose that the state variable $x \in \mathbb{R}^n$ can be used to estimate and discretize the entire control process. Then, the discrete stochastic differential equation is used to express the system state, x_k, and the observation value, z_k:

$$\begin{cases} x_k = Sx_{k-1} + Gu_{k-1} + w_{k-1} \\ z_k = Hx_k + v_k \end{cases}, \tag{20}$$

where u_k is the control vector, S is the state transition matrix, G is a random signal of the control input matrix, H is the state observation matrix, and w_k and v_k are process excitation and observation noises, respectively. Normally distributed white Gaussian noises can be obtained as:

$$\begin{cases} w_k = N(0,\ M_k) \\ v_k = N(0,\ O_k) \end{cases}, \tag{21}$$

where M_k and O_k are the covariance matrices of the process excitation and observation noises, respectively.

The predicted value of the system state, $\overline{x}_{\overline{k}}$, and the optimal estimate of the state, $\overline{x}_k$, can be expressed as:

$$\begin{cases} \overline{x}_{\overline{k}} = S\overline{x}_{k-1} + Gu_k \\ \overline{x}_k = \overline{x}_{\overline{k}} + K_k\left(z_k - H\overline{x}_{\overline{k}}\right) \end{cases}, \tag{22}$$

because the estimation principle of the Kalman filter is to minimize D_k, the covariance of $\overline{x}_k$, making it increasingly close to the true value. Then, the cost function, J_k, is established:

$$J_k = \sum\nolimits_{min} D_k \tag{23}$$

By combining Equations (22) and (23), the filter gain of the Kalman filter, estimation error variance, and state estimation covariance are calculated:

1. Kalman filter gain:

$$K_k = D_k^- H^T\left(HD_k^- H^T + O_k\right)^{-1}. \tag{24}$$

2. Estimation error variance:

$$D_k = (E - K_k H_k)D_k^-. \tag{25}$$

3. State estimation covariance:

$$D_{k+1}^- = SD_k S^T + M_k. \tag{26}$$

2.2.4. Sideslip Angle Observer

Based on the linear two-degrees-of-freedom vehicle model and the Kalman filter, the state and measurement equations of the sideslip angle observer are obtained:

$$\begin{cases} F = \begin{bmatrix} \frac{C_f+C_r}{mv_x} & \frac{aC_f-bC_r}{mv_x^2}-1 \\ \frac{aC_f-bC_r}{I} & \frac{a^2C_f+b^2C_r}{Iv_x} \end{bmatrix} + \begin{bmatrix} -\frac{C_f}{mv_x} \\ -\frac{aC_r}{I} \end{bmatrix} \delta_f \\ W = \begin{bmatrix} \frac{C_f+C_r}{m} & \frac{aC_f-bC_r}{mv_x} \\ 0 & 1 \end{bmatrix} + \begin{bmatrix} -\frac{C_f}{m} \\ 0 \end{bmatrix} \delta_f \end{cases}. \quad (27)$$

Thus, the initial state of the system is obtained:

$$F = \begin{bmatrix} 0 & 0 \end{bmatrix}. \quad (28)$$

2.3. Hardware-in-the-Loop Test

The effectiveness of the proposed LKAS control strategy was verified by the hardware-in-the-loop test, where the test bench consisted of six main components: upper computer, lower computer, interface system, steering column, steering motor controller, and servo motor controller. In the upper computer, the TruckSim 2019 (Mechanical Simulation Corp., Ann Arbor, MI, USA) vehicle dynamics, road environment, and Matlab/Simulink R2016a (MathWorks, Natick, MA, USA) control models were established. The linear two-degrees-of-freedom vehicle dynamics model and the vehicle lateral tracking deviation model were used in the control algorithm built in Matlab/Simulink. The vehicle dynamic model was selected from the model base provided by TruckSim, the parameters of the vehicle model are listed in Table 1, and the road model was designed as discussed in Section 2.1.1. The longitudinal vehicle speed, lateral acceleration, and preview deviation were obtained from the TruckSim vehicle model. Matlab/Simulink and TruckSim were connected and interacted in the VeriStand 2017 environment (National Instruments Corp., Austin, TX, USA). The lower computer utilized the National Instruments PXI system to run the real-time simulation program created by the upper computer. The interface system transmitted the steering angle calculated by the LKAS control strategy to the servo motor controller through controller area network signals. The servo motor controller converted the received data into hexadecimal format and sent this to the steering motor to control the steering angle. Simultaneously, the steering angle signal acquired by the steering wheel angle sensor was input to the PXI real-time system. The hardware-in-the-loop process flowchart is shown in Figure 6.

Table 1. Vehicle parameters.

Parameters	Values
Vehicle mass, m (kg)	5760
Moment of inertia along z-axis, I_z (kg·m^2)	348,23.2
Equivalent side stiffness of front tires, C_f (N·rad^{-1})	259,752
Equivalent side stiffness of rear tires, C_r (N·rad^{-1})	259,752
Distance from center of mass to front axle, a (m)	1.25
Distance from center of mass to rear axle, b (m)	3.75

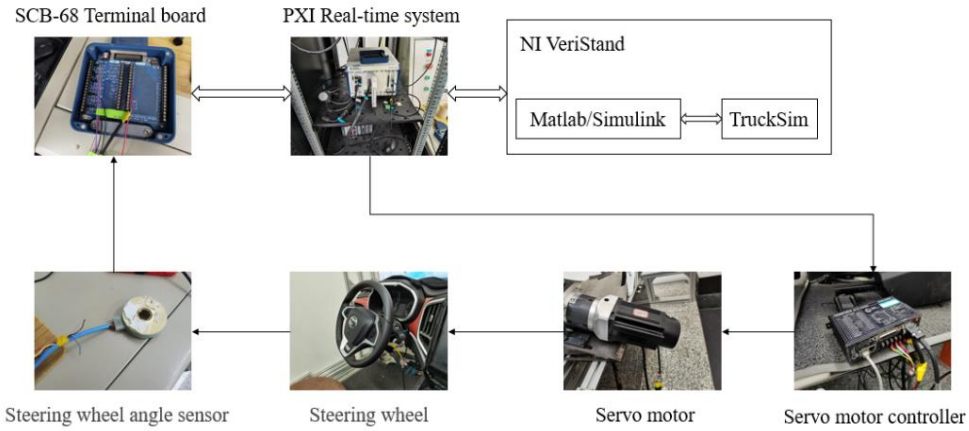

Figure 6. Hardware-in-the-loop flowchart.

3. Results

The lateral stability performance of the vehicle was judged by comparing the sideslip angle, yaw rate, and lateral acceleration during driving, because they are important parameters to characterize the lateral stability of the vehicle, and whether the vehicle is in a stable state during driving can be seen through these parameters.

In the first condition, without crosswind, that was under normal driving conditions without any lateral interference, the LKAS strategy could control the vehicle to track the target path on the test road, so that the vehicle was kept in the middle of the road line, where the vehicle was driven at a speed of 80 km/h. As shown in Figure 7, from 4 s to 20 s, the vehicle was on the curved part of the test road and was constantly adjusting its position, so the lateral position deviation was also increased with the continuous changes. However, the LKAS control strategy can maintain the accuracy of the lateral position deviation at the millimeter level, and the vehicle was smoothly kept in the middle of the road line. Therefore, the designed LKAS control strategy exhibited high precision.

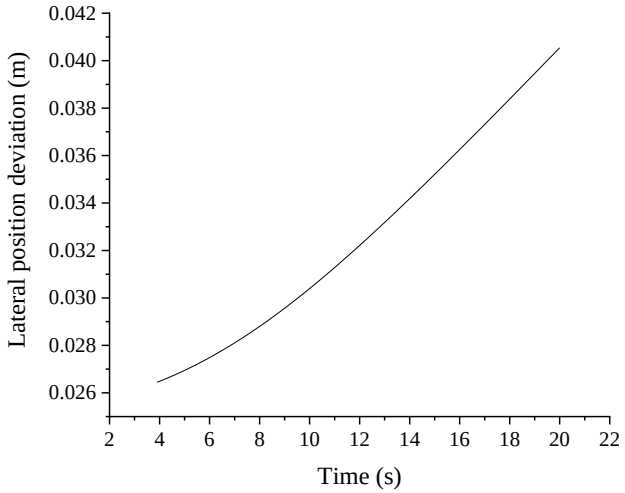

Figure 7. Vehicle lateral position deviation.

In the other conditions, when the crosswind interference was considered, the LKAS strategy controlled the vehicle to track the target path on the test road, so that the vehicle remained in the middle of the road line, the maximum crosswind speed was 40 km/h, and the vehicle was traveling at 80 km/h. As shown in Figure 8, The vehicle began to enter the curve at 4 s after being affected by the crosswind. However, the steering angle quickly adjusted after 0.1 s, enabling the vehicle to continue tracking the path with high precision. The maximum steering angle with LQR control was 30° during the crosswind

disturbance, while the maximum steering angle without LQR control reached 40°. After leaving the crosswind zone, the vehicle with LQR control quickly stabilized to 19° after 1 s, while the vehicle without LQR control continued to oscillate. The sideslip angle, yaw rate, and lateral acceleration of the vehicle are shown in Figures 9–11, respectively. As shown in Figure 9, the sideslip angle of the vehicle using the LQR control strategy had a significant adjustment and changed quickly, and the amplitude change of the lateral acceleration was smaller than that of the vehicle without the use of LQR control. Then, starting from the 6th second, the interference of crosswind disappeared, and the vehicle without the LQR control strategy had a large fluctuation, so the vehicle was in an unstable state. As show in Figure 10, when the crosswind disappeared from the 6th second, the rapidly rising lateral acceleration was quickly pulled back to 0.1 m/s^2 and became stable. As shown in Figure 11, the yaw rate of the LQR-controlled vehicle responded quickly after encountering the crosswind in the 4th second, and after leaving the crosswind zone, the yaw rate rapidly became stable. Meanwhile, the compared parameters of the vehicle without LQR control were slow to respond when it encountered crosswind interference at 4 s, and the amplitude of the adjustment was higher. After leaving the crosswind area, the vehicle did not quickly enter a stable state but kept oscillating, so the vehicle was in an unstable state. Therefore, by comparing the differences in the sideslip angle, lateral acceleration, and yaw rate of the vehicle when driving on a curved road while being disturbed by crosswinds, it can be seen that the LQR control strategy can ensure that the vehicle can drive smoothly on the test road when disturbed by crosswinds, without instability, which further proves the effectiveness of the designed LKAS control strategy.

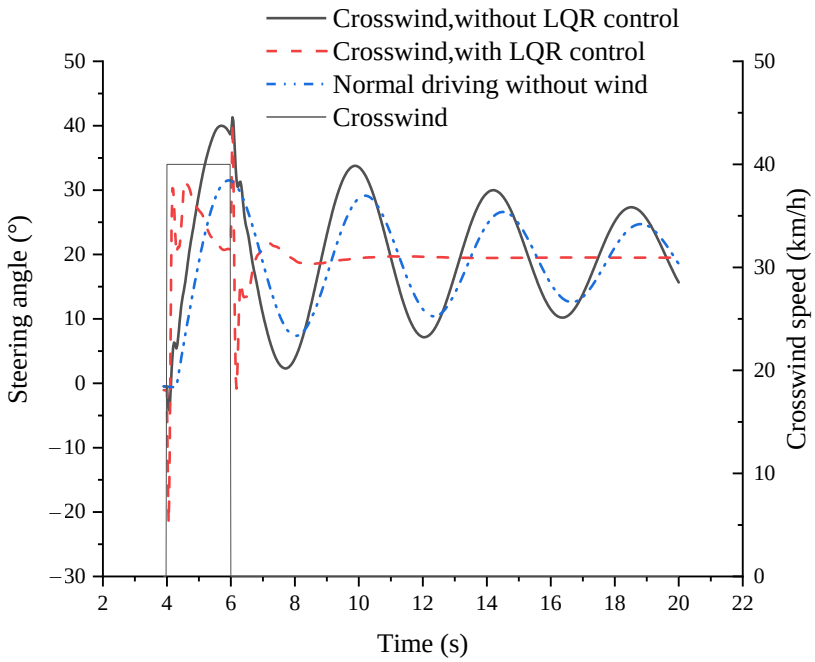

Figure 8. Steering angle.

Figure 12 presents the experimental results of the desired and actual steering angles. A slight deviation between the desired and actual steering angles can be observed, which is attributed to the presence of friction in the real steering system and the time response of the motor. Therefore, in the future, it is necessary to conduct actual vehicle tests to further test the feasibility of the LKAS control strategy.

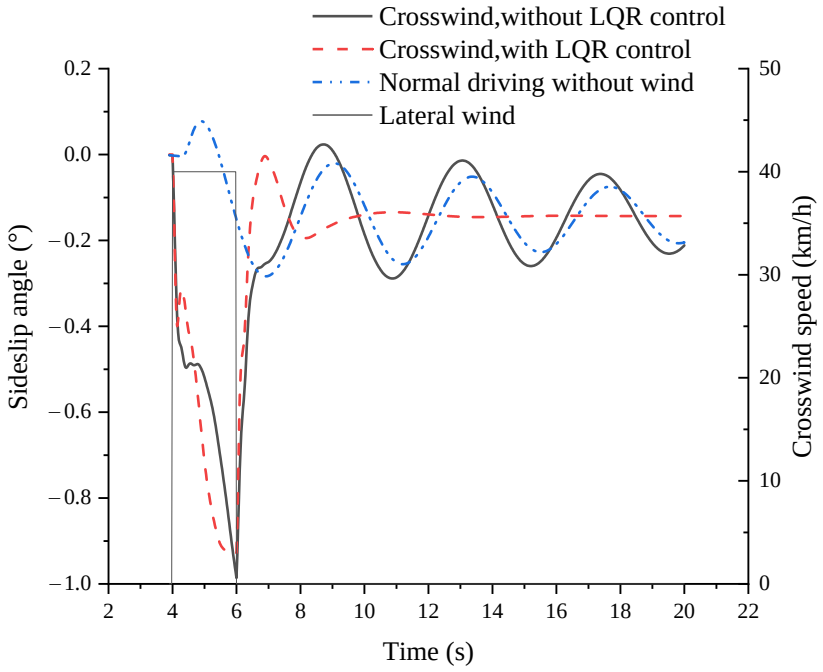

Figure 9. Sideslip angle.

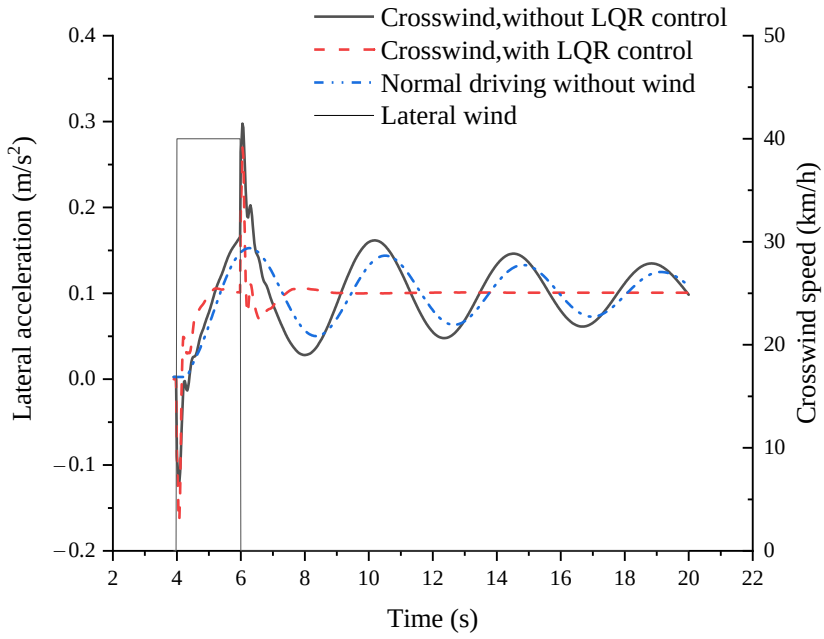

Figure 10. Lateral acceleration.

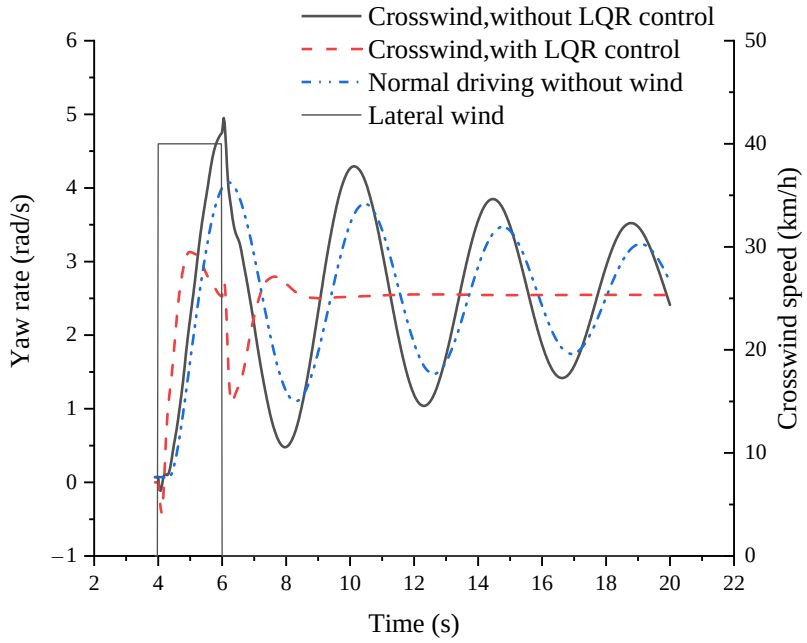

Figure 11. Yaw rate.

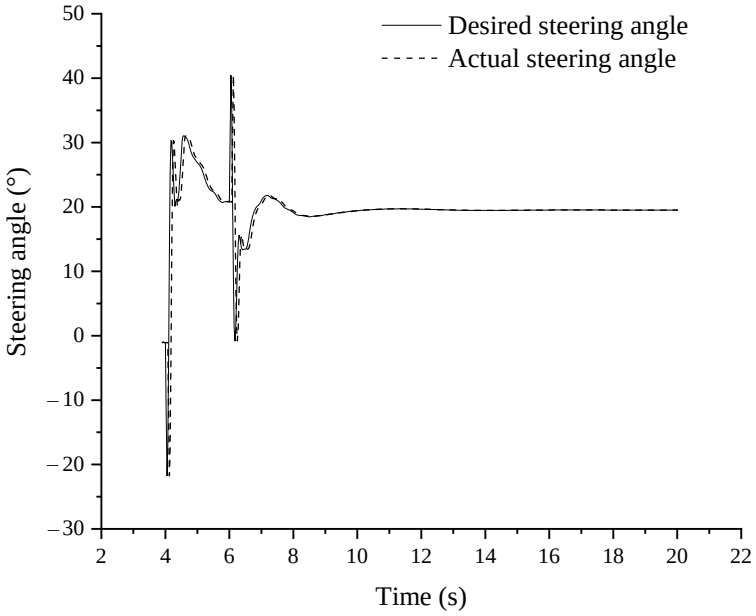

Figure 12. Desired and actual steering angles.

4. Discussion

This study focused on the use of a LKAS control strategy in crosswind environments to control vehicles to drive smoothly in the middle of the road lines on straight and curved composite roads. Through the test results, it can be seen that when the vehicle entered the curve at the 4th second and encountered crosswind, the sideslip angle and lateral acceleration of the vehicle with LQR control were more stable and less fluctuating than those without LQR control, and the yaw rate changed less and more smoothly with LQR control, which increased by 66.7% compared to without LQR control, thereby improving the lateral stability of the vehicle in the crosswind environment.

However, due to the limitations of the conditions, there are still some shortcomings in the safety analysis of trucks, mainly because this study used step wind, whereas the

actual crosswind environment is mostly unstable wind, the wind strength on the vehicle is different at different times and seasons, and there are environmental problems including rainy days, snow days, etc., which have a greater impact on the safety of trucks. In future experimental research, it is necessary to build a more reasonable, effective, and realistic simulation environment, conduct more detailed experiments, and analyze the results, to further improve the theoretical system.

5. Conclusions

This study proposed an LKAS control strategy based on the LQR. To determine the appropriate front wheel steering angle and enable the vehicle to smoothly remain in the center of the lane under crosswind conditions, a path-tracking preview algorithm was used to calculate the lateral position deviation. However, this method did not yield satisfactory control results under complex conditions with boundary constraints. Therefore, an LQR algorithm was established for optimal control. However, optimization resulted in steady-state errors. Thus, a feedforward controller based on the LQR and a linear two-degrees-of-freedom vehicle model were developed to eliminate the steady-state errors. To achieve more accurate control, a sideslip angle observer based on the Kalman filter and a lateral tracking deviation model of the vehicle were used to estimate the sideslip angle and yaw rate deviations. The proposed control strategy was verified through a combination of simulations using TruckSim and Matlab/Simulink and hardware-in-the-loop experiments. The results demonstrated that the method effectively kept the vehicle in the center of the lane under crosswind conditions, indicating robust performance. However, no actual vehicle testing was conducted here, and further research is needed on the application of the LKAS control strategy in actual vehicles.

Author Contributions: Conceptualization, C.L. and L.H.; methodology, H.L. and C.L.; software, H.L.; validation, H.L.; investigation, H.L. and D.Z.; writing—original draft preparation, H.L.; writing—review and editing, D.Z.; supervision, C.L.; funding acquisition, L.H. and C.L. All authors have read and agreed to the published version of the manuscript.

Funding: This research was funded by the Liaoning Province Higher Education Intercollegiate Cooperation Project, grant number 2021-21.

Institutional Review Board Statement: Not applicable.

Informed Consent Statement: Not applicable.

Data Availability Statement: Not applicable.

Conflicts of Interest: The authors declare no conflict of interest.

References

1. Zachiotis, A.T.; Giakoumis, E.G. Monte Carlo simulation methodology to assess the impact of ambient wind on emissions from a light-commercial vehicle running on the worldwide-harmonized light-duty vehicles test cycle (WLTC). *Energies* **2021**, *14*, 661. [CrossRef]
2. Sekulic, D.; Vdovin, A.; Jacobson, B.; Sebben, S.; Johannesen, S.M. Effects of wind loads and floating bridge motion on intercity bus lateral stability. *J. Wind Eng. Ind. Aerodyn.* **2021**, *212*, 104589. [CrossRef]
3. Han, Y.; Huang, J.; Cai, C.S.; Chen, S.; He, X. Driving safety analysis of various types of vehicles on long-span bridges in crosswinds considering aerodynamic interference. *Wind Struct.* **2019**, *29*, 279–297. [CrossRef]
4. Xu, L.; Zhai, W.M. The vehicle-track stochastic model considering joint effects of cross-winds and track random irregularities. *J. Vib. Eng.* **2018**, *31*, 39–48.
5. Kim, K.; Kim, B.; Go, Y.; Park, J.; Suh, I.; Yi, K. An investigation on motor-driven power steering-based crosswind disturbance compensation for the reduction of driver steering effort. *Veh. Syst. Dyn.* **2014**, *52*, 922–947. [CrossRef]
6. Cioffi, A.; Prakash, A.R.; Sabbioni, E.; Vignati, M.; Cheli, F. Heavy-vehicle response to crosswind: Evaluation of driver reactions using a dynamic driving simulator. *Vehicles* **2023**, *5*, 344–366. [CrossRef]
7. Tian, G.; Jia, Y.; Chen, Z.; Gao, Y.; Wang, S.; Wei, Z.; Chen, Y.; Zhang, T. Evaluation on lateral stability of vehicle: Impacts of pavement rutting, road alignment, and adverse weather. *Appl. Sci.* **2023**, *13*, 3250. [CrossRef]
8. Bian, Y.; Ding, J.; Hu, M.; Xu, Q.; Wang, J.; Li, K. An advanced lane-keeping assistance system with switchable assistance modes. *IEEE Trans. Intell. Transp. Syst.* **2020**, *21*, 385–396. [CrossRef]

9. Kim, W.; Son, Y.S.; Chung, C.C. Torque-overlay-based robust steering wheel angle control of electrical power steering for a lane-keeping system of automated vehicles. *IEEE Trans. Veh. Technol.* **2016**, *65*, 4379–4392. [CrossRef]
10. Chen, W.; Zhao, L.; Wang, H.; Huang, Y. Parallel distributed compensation/H_∞ control of lane-keeping system based on the Takagi-Sugeno fuzzy model. *Chin. J. Mech. Eng.* **2020**, *33*, 61. [CrossRef]
11. Zhang, X.; Yang, W.; Tang, X.; Wang, Y. Lateral distance detection model based on convolutional neural network. *IET Intell. Transp. Syst.* **2019**, *13*, 31–39. [CrossRef]
12. Zhou, X.; Shen, H.; Wang, Z.; Ahn, H.; Wang, J. Driver-centric lane-keeping assistance system design: A noncertainty-equivalent neuro-adaptive control approach. *IEEE/ASME Trans. Mechatron.* **2023**, *Unpublished, Early Access*. [CrossRef]
13. Wu, Y.; Zhu, Y.; Li, F. Electric vehicle lane keeping assistance system based on active torque distribution. *Sci. Technol. Rev.* **2018**, *36*, 98–104.
14. Han, X.; Zhao, W.; Zheng, H.; Yu, L. Research on lane-keeping control strategy for bus. *Int. J. Heavy Veh. Syst.* **2019**, *26*, 291–314. [CrossRef]
15. Lim, H.; Kim, C.; Yi, K.; Jeon, K. Design and implementation of human driving data-based lane-keeping assistance system for electric bus. *Proc. Inst. Mech. Eng. Part D J. Automob. Eng.* **2022**, *236*, 3005–3026. [CrossRef]
16. Kővári, B.; Hegedüs, F.; Bécsi, T. Design of a reinforcement learning-based lane keeping planning agent for automated vehicles. *Appl. Sci.* **2020**, *10*, 7171. [CrossRef]
17. *GB/T 41796-2022*; Performance Requirements and Test Methods for Lane-Keeping Assistance System of Commercial Vehicles. State Administration for Market Regulation: Beijing, China, 2022.
18. Huang, T.; Gu, Z.; Feng, C.; Zeng, W. Transient aerodynamics simulations of a road vehicle in the crosswind condition coupled with the vehicle's motion. *Proc. Inst. Mech. Eng. Part D J. Automob. Eng.* **2018**, *232*, 583–598. [CrossRef]
19. Cai, Y.-F.; Zang, Y.; Sun, X.-Q.; Chen, X.-B.; Chen, L. Lane-keeping system of intelligent vehicles based on extension switching control method. *China J. Highw. Transp.* **2019**, *32*, 43–52. [CrossRef]
20. Kudinov, Y.I.; Pashchenko, F.F.; Kelina, A.Y.; Vasutin, D.I.; Duvanov, E.S.; Pashchenko, A.F. Analysis of control system models with conventional LQR and fuzzy LQR controller. *Procedia Comput. Sci.* **2019**, *150*, 737–742. [CrossRef]
21. Zhao, C.; Zhang, C.; Guo, F.; Shao, Y. Research on path following control method of agricultural machinery autonomous navigation through LQR-feed forward control. In Proceedings of the 2021 IEEE International Conference on Data Science and Computer Application (ICDSCA), Dalian, China, 29–31 October 2021; pp. 228–233. [CrossRef]
22. Welch, G.; Bishop, G. *An Introduction to the Kalman Filter*; University of Carolina at Chapel Hill: Chapel Hill, NC, USA, 1995.